Hindawi Publishing Corporation
Journal of Nanomaterials
Volume 2014, Article ID 462356, 13 pages
http://dx.doi.org/10.1155/2014/462356

Research Article

Development, Characterization, and Evaluation of PSMA-Targeted Glycol Chitosan Micelles for Prostate Cancer Therapy

Jing Xu,[1,2,3] Jingmou Yu,[1] Xiao Xu,[2] Liangliang Wang,[2] Yonghua Liu,[2] Lixin Li,[1] Jianguo Zhao,[1] and Ming He[3]

[1] *College of Basic Medical Science, Jiujiang University, Jiujiang, Jiangxi 332000, China*
[2] *Affiliated Hospital of Jiujiang University, Jiujiang, Jiangxi 332000, China*
[3] *Medical Department of Graduate School, Nanchang University, Nanchang, Jiangxi 33006, China*

Correspondence should be addressed to Jingmou Yu; yjm1016@hotmail.com

Received 20 July 2014; Revised 6 October 2014; Accepted 6 October 2014; Published 15 October 2014

Academic Editor: Hongchen Chen Gu

Prostate cancer-binding peptides- (PCP-) modified polymeric micelles were prepared and used for the treatment of prostate-specific membrane antigen- (PSMA-) expressing prostate cancer in a target-specific manner. Cholesterol-modified glycol chitosan (CHGC) was synthesized. PCP-conjugated CHGC (PCP-CHGC) micelles were fabricated and characterized. The degree of substitution was 5.2 PCP groups and 5.8 cholesterol groups per 100 sugar residues of glycol chitosan. The critical aggregation concentration (CAC) of PCP-CHGC copolymer was 0.0254 mg/mL. Doxorubicin (DOX) was chosen as a model antitumor drug. The DOX-loaded micelles were prepared by an o/w method. The mean diameter of DOX-loaded PCP-CHGC (DOX-PCP-CHGC) micelles was 293 nm determined by dynamic light scattering (DLS). DOX released from drug-loaded micelles was in a biphasic manner. DOX-PCP-CHGC micelles exhibited higher cytotoxicity *in vitro* against PSMA-expressing LNCaP cells than DOX-loaded CHGC (DOX-CHGC) micelles. Moreover, the cellular uptake of DOX-PCP-CHGC micelles determined by confocal laser scanning microscopy (CLSM) and flow cytometry was higher than that of DOX-CHGC micelles in LNCaP cells. Importantly, DOX-PCP-CHGC micelles demonstrated stronger antitumor efficacy against LNCaP tumor xenograft models than doxorubicin hydrochloride and DOX-CHGC micelles. Taken together, this study provides a potential way in developing PSMA-targeted drug delivery system for prostate cancer therapy.

1. Introduction

Prostate cancer is one of the most frequently diagnosed cancers among men in the United States and is the second leading cause of male cancer death with 233,000 new cases and an estimated 29,480 deaths in 2014 [1]. Current treatment for prostate cancer commonly involves surgery, radiation therapy, hormone administration, and/or chemotherapy [2, 3]. In the early stage of prostate cancer, the surgical or radiation ablation therapies are relatively effective. Unfortunately, there is no effective therapy for men with metastatic prostate cancer. Clinical data have exhibited that chemotherapeutic agents may prolong survival in a subset of patients. Nevertheless, the dose and duration of administration of these drugs were limited, due to the systemic toxicity and the lack of sufficient selectivity towards tumor cells. Thus, it is an urgent medical need to develop drug delivery systems that selectively transport the antitumor agent into the tumor tissues and cells. Nanosized carriers such as liposomes, micelles, and polymeric nanoparticles have demonstrated improved therapeutic index with minimal side effects [4–6].

In recent years, polymeric micelles have received much attention, particularly due to the great potential as drug delivery vehicles in cancer chemotherapy [7–10]. The amphiphilic copolymers can spontaneously form nanostructures with hydrophobic cores and a hydrophilic outer shell in aqueous medium. The hydrophobic core can act as the drug-loading depot, while the surrounding hydrophilic shell can increase

stabilization. Moreover, the micelles possess unique properties such as increasing blood circulation time *in vivo* and passive accumulation in tumor tissue by the enhanced permeability and retention (EPR) effect [11–13]. In particular, the biodegradable and nontoxic polymeric conjugates, such as glycol chitosan-based amphiphiles, attracted considerable interests [14–16]. Glycol chitosan self-assembled nanoparticles demonstrated high tumor accumulation that was useful for *in vivo* delivery of hydrophobic drugs or genes [17–19]. In our previous study, amphiphilic cholesterol-modified glycol chitosan (CHGC) was synthesized and formed aggregated nanoparticles in aqueous solution [20]. Moreover, the DOX-loaded CHGC nanoparticles showed the prolonged circulation in blood and exhibited stronger antitumor activity against S180 tumor-bearing mice by the EPR effect than doxorubicin hydrochloride. Further, the nanoparticle surface can be functionalized to attain active targeting, leading to improvement of drug intratumoral accumulation. This can be achieved by tagging target-specific moieties or ligands onto the micelle's surface [21–23]. Such ligands are recognized by specific receptors which are either uniquely expressed or overexpressed on certain types of cancer cell surfaces. Several targeting moieties, such as folate, aptamer, or peptides, have been successfully conjugated with the carriers to deliver antitumor drugs or genes for treatment of prostate cancer [24–26].

One promising candidate for targeted prostate cancer therapy is prostate-specific membrane antigen (PSMA), a 100 kDa membrane-bound glycoprotein, which is highly overexpressed on the surface of human prostate cancer cell lines (such as LNCaP and CWR22R) and tumor-associated neovasculature in a variety of solid tumors [27, 28]. In prostate cancer tissues, PSMA is expressed at levels > 1000-fold greater than that in other tissues, such as brain and proximal small intestines [29]. Hence, extensive efforts have been devoted to investigating PSMA receptor binding ligands [3]. For example, the peptide phage display approach has been widely used to search for ligands that bind epitopes on the cell surfaces *in vitro* and *in vivo*. Romanov et al. performed search for peptide ligands to PSMA-expressing LNCaP cells receptors, and they found that the prostate cancer-binding peptides (DPRATPGS sequence) were the best binder to the surfaces of LNCaP cells [30]. Based on the above considerations, we attempted to use PCP as the targeting moiety to fabricate targeted drug delivery system.

Herein, the purpose of this study was to develop PSMA-targeted polymeric micelles for prostate cancer therapy. PCP-modified CHGC conjugate was synthesized and characterized. The physicochemical properties of PCP-CHGC micelles were then investigated. DOX, a typical cytotoxic anthracycline antibiotic, was chosen as antitumor model drug and encapsulated into the PCP-CHGC micelles. Further, *in vitro* cellular uptake and cytotoxicity of DOX-load micelles were evaluated in prostate cancer cell lines, LNCaP and PC-3. The antitumor efficacy studies of drug-loaded micelles were also investigated in LNCaP-bearing nude mice.

2. Materials and Methods

2.1. Materials. Glycol chitosan (M_w = 28 kDa) was obtained by enzymatic degradation of 75.2% deacetylated glycol chitosan [31, 32], which was purchased from Wako Pure Chemical Industries, Ltd. (Osaka, Japan). Cholesterol, succinic anhydride, 1-ethyl-3-(3-dimethylaminopropyl)-carbodiimide hydrochloride (EDC), and 4-(*N*-maleimidomethyl)cyclohexanecarboxylic acid *N*-hydroxysuccinimide ester (SMCC) were all provided by Sigma-Aldrich (St. Louis, MO, USA). Potassium poly(vinyl sulfate) was supplied by Wako Pure Chemical Industries, Ltd. (Osaka, Japan). Pyrene was obtained from Acros Organics (New Jersey, USA). The Ac-CDPRATPGS peptide (M_w = 945 Da) was synthesized by GL Biochem Ltd. (Shanghai, China). Doxorubicin hydrochloride (DOX·HCl) was from Beijing Huafeng United Technology Co., Ltd. (Beijing, China). RPMI 1640 medium and trypsin-EDTA were purchased from Jinuo Biotechnology Company (Hangzhou, China). Fetal bovine serum (FBS) was supplied by Hangzhou Sijiqing Biological Engineering Materials Co., Ltd. (Zhejiang, China). 5, 5′-Dithiobis(2-nitrobenzoic acid) and 3-(4,5-dimethylthiazol-2-yl)-2,5-diphenyltetrazolium bromide (MTT) were supplied by Sigma-Aldrich (St. Louis, MO, USA). All other chemicals were of analytical grade.

Male BALB/c nude mice (4 weeks of age, Hunan SLAC Jingda Laboratory Animal Co. Ltd., Changsha, China) were maintained in a pathogen-free condition. All animal experiments were performed according to the international regulations for animal experimentation.

2.2. Synthesis of CHGC Conjugate. CHGC conjugate was synthesized by using our previous method with little modification [31]. Briefly, cholesterol and succinic anhydride were mixed and reacted for 24 h. Then cholesterol hemisuccinate was obtained by purification and recrystallization. Glycol chitosan (500 mg) was dispersed in 30 mL of distilled water overnight and was diluted with 106 mL of ethanol under quick stirring. EDC (58.3 mg) and cholesterol hemisuccinate (74.0 mg) were dropwise added. After 72 h, the mixture was sequentially dialyzed (MWCO: 3.5 kDa) against the excess amount of ethanol/distilled water solution (88 : 12, v/v) and distilled water. Finally, the dialyzed solution was filtered through 0.8 μm membrane and lyophilized to obtain CHGC copolymer.

2.3. Synthesis of PCP-CHGC Conjugate. CHGC (100 mg) was dissolved in 40 mL of distilled water (pH 8.0) and followed by sonication using a probe type sonifier (Ningbo Scientz Biotechnology Co. Ltd., Ningbo, China) at 200 W for 40 times in an ice bath. Then the coupling agent SMCC (10.8 mg) was added, which was dissolved in 0.5 mL of DMSO. The solution was stirred at room temperature for 2 h. After adjusting the pH value of the mixture to 6.8, PCP (Ac-CDPRATPGS sequence, 45.2 mg) were introduced. After further 4-hour reaction, the unconjugated PCP were discarded by using the centrifugal-ultrafiltration method [33]. The resulting solution was dialyzed (MWCO: 3.5 kDa) against distilled water for 24 h. The purified dialysate was freeze-dried and stored at −20°C.

2.4. Preparation of DOX-Loaded Micelles. The DOX-loaded micelles were prepared by the emulsion/solvent evaporation

method [34, 35]. The blank copolymer micelles were prepared by probe sonication as stated above. DOX base was produced by reaction of DOX·HCl with 3-mole equivalent of triethylamine in chloroform overnight. 3 mL of DOX (4.5 mg) solution was added to 60 mL of blank micelles (30 mg, CHGC or PCP-CHGC) under vigorous stirring to form the o/w emulsion. Then the mixture solution was placed into a flask and evaporated under reduced pressure condition, allowing removal of chloroform and formation of self-assembled micelles. The aqueous suspension was filtered through a 0.8 μm membrane and eluted through a Sephadex G25 fine column to remove nonencapsulated DOX. The DOX-loaded micelles were lyophilized and kept at −20°C for future use.

2.5. Characterization. ^{1}H-nuclear magnetic resonance (NMR) spectra were recorded on Avance DMX500 spectrometer using D_2O as the solvent. Chemical shifts are shown in parts per million (ppm).

The cholesterol substitution degree in the conjugates was investigated by a colloidal titration method, which is based on the reaction between positively charged glycol chitosan and negatively charged potassium poly(vinyl sulfate) [15, 36]. Briefly, 5 mg of CHGC was dissolved in 2% acetic acid solution (5 mL) overnight. Then, 100 μL of the indicator and 0.1% (w/v) toluidine blue were added under a stirring condition. The CHGC suspension was slowly titrated with 2.5 mM potassium poly(vinyl sulfate) solution until the opaque solution suddenly became clear. Another 5 mL of distilled water was used as blank assay.

The substitution degree of PCP in the PCP-CHGC conjugate was measured by Ellman's assay, which can detect free sulfhydryl groups in solution. After the synthesis reaction, the unconjugated prostate cancer-binding peptides were removed by the centrifugal-ultrafiltration method. Thereafter, the unreacted PCP or initially fed PCP was dissolved in Ellman's working solution. Ellman's reagent solution was immediately added and stirred for 15 min at room temperature. After filtration, the solution was measured by ultraviolet spectrometer (UV-1206, Shimadzu Corp., Japan) with the absorbance at 412 nm. The amounts of unattached PCP and initially fed PCP were determined. Then the amount of PCP groups conjugated to PCP-CHGC was calculated by the subtraction method.

The critical aggregation concentration (CAC) of micelles was investigated by using pyrene as a florescent probe. The PCP-CHGC conjugate suspension was prepared by sonication as described above and adjusted to various conjugate concentrations. A known amount of pyrene in acetone was added into each of the 10 mL vials, and acetone was evaporated. A total of 10 mL of various concentrations of PCP-CHGC conjugate were introduced into each vial and heated at 50°C for 10 h to equilibrate pyrene and the micelles. And the mixture solution remained undisturbed to cool overnight at room temperature. The final concentration of pyrene was 6.0×10^{-7} M. Steady-state fluorescent spectra were measured using a fluorescence spectrophotometer (Hitachi F-4500, Japan). The excitation and emission wavelengths were set at 339 and 390 nm, respectively. The slit width was 2.5 nm.

The hydrodynamic diameters of the micelles were determined by dynamic light scattering (90Plus, Brookhaven Instruments Corp., Holtsville, NY, USA). Transmission electron microscopy (TEM, JEM-1230, Japan) was employed to observe the morphology of the micelles at an acceleration voltage of 80 kV. TEM sample was prepared by placing a drop of micelles onto a 300-mesh copper grid coated with carbon. The extra solution was blotted with filter paper, followed by air drying.

The DOX-loading content (LC) and entrapment efficiency (EE) of DOX-loaded micelles were investigated by using a UV-Vis spectrophotometer (UV-1206, Shimadzu Corp., Japan). The freeze-dried samples were dispersed in aqueous solution, and DMSO was added to dissociate the micelles. The absorbance at 481 nm was performed to detect the DOX concentration. The LC and EE were calculated by

$$\text{LC}\,(\%) = \frac{\text{the amount of DOX in micelles}}{\text{total amount of DOX-loaded micelles}} \times 100,$$
$$\text{EE}\,(\%) = \frac{\text{the amount of DOX in micelles}}{\text{the amount of DOX fed initially}} \times 100. \quad (1)$$

2.6. In Vitro Drug Release. *In vitro* release studies of DOX from DOX-loaded micelles were investigated in phosphate-buffered saline (PBS) (pH 7.4). Briefly, 1 mL of DOX-loaded micelles solution was added into a dialysis bag (MWCO: 3.5 kDa) and put into a plastic tube containing 20 mL of PBS solution. The tubes were kept at 37°C in a thermostated shaker at 100 rpm. At selected time intervals, the release medium outside the dialysis bag was totally withdrawn and replaced with the same volume of fresh PBS solution. The DOX concentration was determined by fluorescence spectrophotometer. All drug-release tests were performed in triplicate.

2.7. Cell Culture. LNCaP and PC-3 cells were obtained from the Cell Bank of Shanghai Institutes for Biological Sciences, Chinese Academy of Sciences (Shanghai, China), and grown in RPMI-1640 medium containing 10% FBS and 1% penicillin-streptomycin. The cells were maintained in a 37°C humidified incubator with 5% CO_2 atmosphere. LNCaP cells were specially cultured in CellBIND flasks or plates (Costar, Corning, NY, USA).

2.8. In Vitro Cellular Uptake. In order to observe the cellular uptake of DOX by LNCaP cells, a confocal fluorescent microscopy was adopted. Briefly, LNCaP cells were seeded at a density of 5×10^5 cells/well in 6-well plates for 48 h until total adhesion was achieved. Then the medium was removed, and DOX·HCl, DOX-CHGC, or DOX-PCP-CHGC micelles (final DOX concentration: 10 μg/mL) in RPMI 1640 medium supplemented with 10% FBS were added. After another 4 hours of incubation, the cells were washed with cold PBS thrice and fixed with 4% paraformaldehyde for 10 min. Finally, the cells were imaged and analyzed by using a Zeiss LSM-510 confocal microscope (Jena, Germany).

The flow cytometry analysis was employed to estimate the cellular uptake of different DOX formulations. Typically,

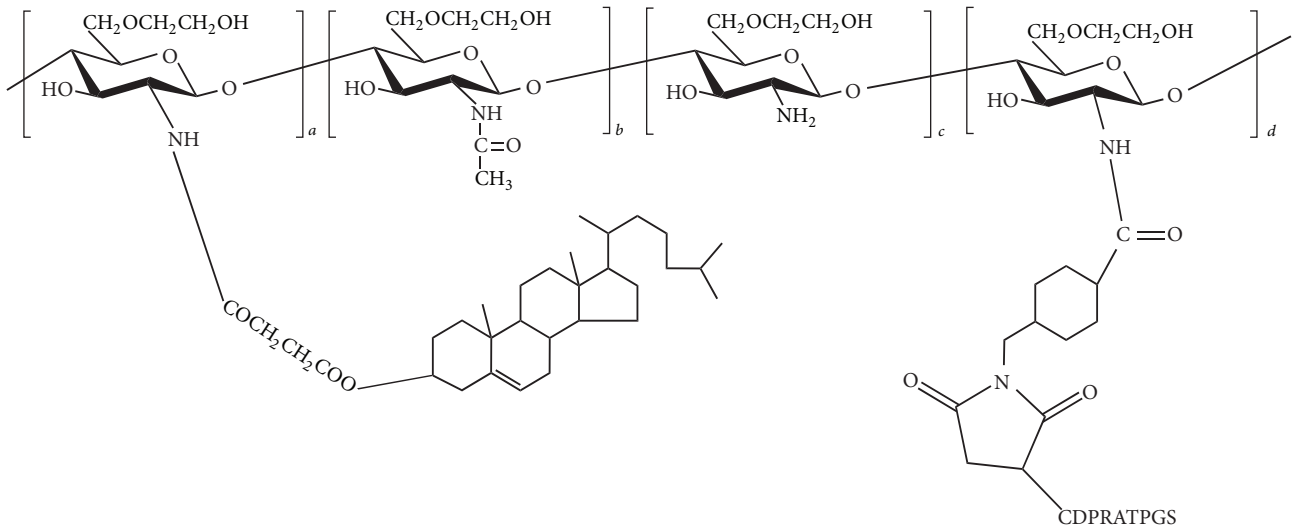

Figure 1: Chemical structure of PCP-CHGC conjugate.

LNCaP cells were seeded at a density of 1×10^6 cells/well in 6-well plates. After the cells were allowed to adhere for 48 h, the medium was replaced with DOX·HCl, DOX-CHGC, or DOX-PCP-CHGC micelles (equivalent DOX concentration: 10 μg/mL) in RPMI 1640 medium supplemented with 10% FBS. After 4 h treatment, the cells were rinsed with cold PBS (pH 7.4), subsequently detached by trypsinization. Then, the cells were resuspended with PBS before the DOX fluorescence intensity was determined using a flow cytometer (Becton Dickinson FACSCalibur, USA) equipped with 488 nm argon ion laser. The data were the mean fluorescent signals for 10,000 cells. Each experiment was conducted in three times.

2.9. In Vitro Cytotoxicity. The *in vitro* cytotoxicity of free DOX, blank micelles, and DOX-loaded micelles was investigated by MTT assay in PSMA-positive LNCaP and PSMA-negative PC-3 cells. Briefly, the cells were plated in 96-well plates at a density of 1×10^5 cells/well and cultured to allow them to adhere at the bottom of the plates. Then, different concentrations of blank micelles, DOX·HCl, or DOX-loaded micelles were added and further incubated for 24 h. After that, the medium in each well was discarded. 200 μL of fresh medium and 30 μL of MTT solution with a concentration of 5 mg/mL were added and incubated for further 4 h at 37°C. Thereafter, the solution was removed and 100 μL of DMSO was added to dissolve MTT formazan crystals. After 15 min incubation, the absorbance of formazan product was measured at 570 nm in a microplate reader (Thermo Scientific Multiskan MK3, Hudson, USA). All the experiments were performed in triplicate.

2.10. In Vivo Tumor Inhibition Study. *In vivo* antitumor efficacy of DOX-PCP-CHGC micelles was assessed in LNCaP tumor xenograft model. Firstly, 1×10^7 cells were suspended in 200 μL of the mixture of Matrigel Matrix (BD Biosciences, San Jose, CA) and RPMI 1640 medium (1 : 1, v : v) and then injected subcutaneously in the right flank of BALB/c nude mice. When the tumor volume was approximately 100 mm^3, the mice were randomly divided into 6 groups ($n = 5$). Animals were treated with 5% glucose injection, DOX·HCl (2.5 mg/kg), DOX-CHGC (2.5 mg/kg on DOX basis), DOX-PCP-CHGC (2.5 mg/kg on DOX basis), CHGC (25 mg/kg), and PCP-CHGC (25 mg/kg) by intravenous injection on days 0, 4, 8, 12, and 16. After the first dose, the mice weight and tumor growth were monitored at a frequency of every 2 days. The tumor size was measured using vernier calipers, and tumor volume was calculated as [0.5 × (length) × (width)^2]. On the 20th day of the therapy, mice were euthanized and the tumors were collected. Then the organs were fixed with paraformaldehyde for 48 h and embedded in paraffin. The sections were stained with hematoxylin and eosin (H&E) to assess the antitumor activity of different treatments via optical microscope observation (Nikon 80i, Japan).

2.11. Statistical Analysis. Data were described using the mean ± standard deviation (SD). The statistical analysis was performed by a one-way ANOVA with a Bonferroni post hoc test. The level of significance was set as $P < 0.05$.

3. Results and Discussion

3.1. Synthesis and Characterization of PCP-CHGC. The chemical structure of PCP-CHGC was shown in Figure 1. Before the PCP modification, the CHGC was synthesized by the reaction between carboxyl group of cholesterol hemisuccinate and amino group of glycol chitosan using EDC as the coupling reagent. And the chemical structure of CHGC was confirmed by ^{1}H NMR spectra (Figure 2). Compared with glycol chitosan, the new signal at 1.27 ppm belonged to methene hydrogen of cholesterol hemisuccinate group, indicating that CHGC conjugate was successfully synthesized [31, 32]. According to the colloidal titration test, the degree of substitution was 5.8 cholesterol groups per 100 sugar residues of glycol chitosan. In addition, PCP groups were conjugated

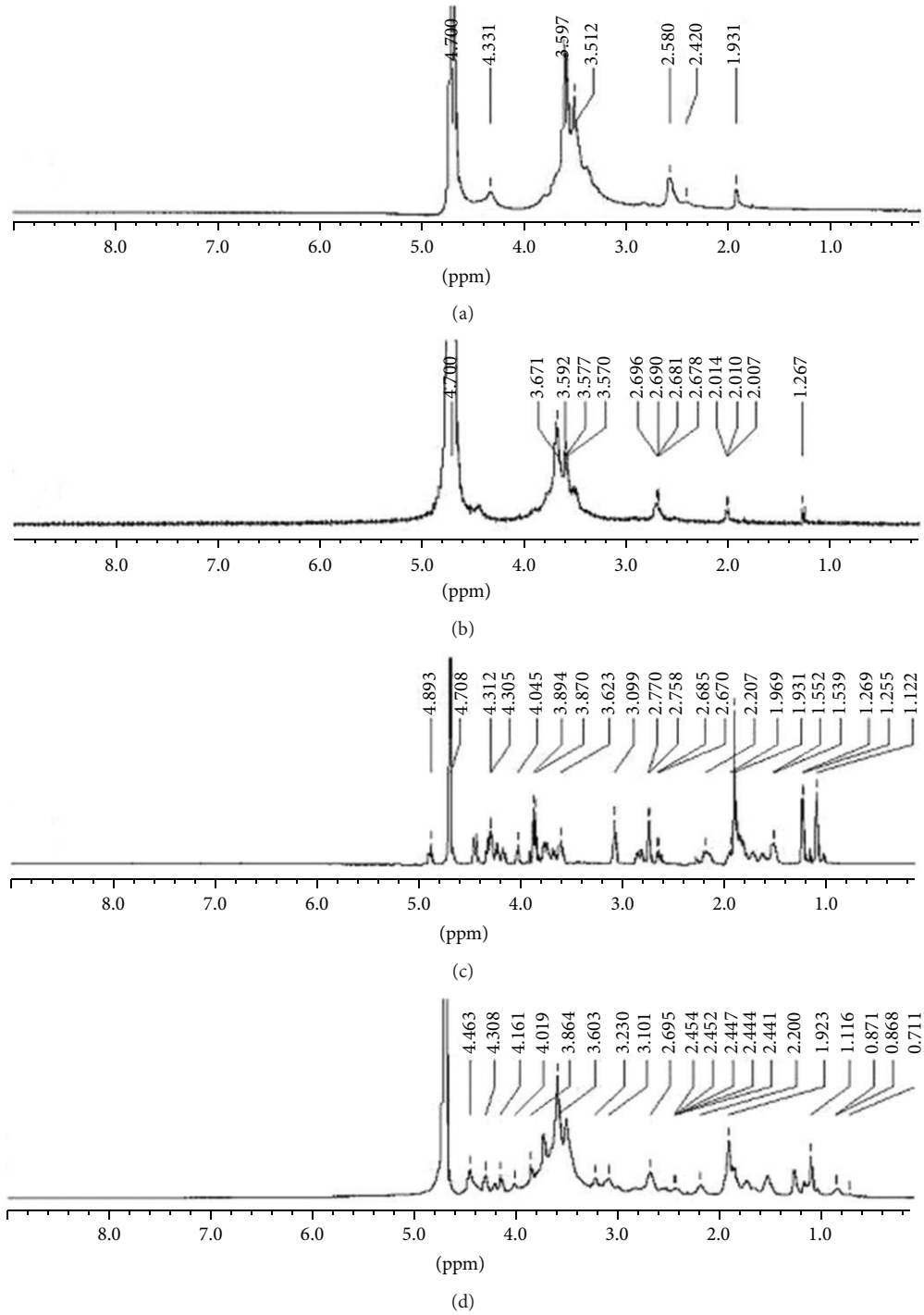

Figure 2: ^{1}H NMR spectra of (a) glycol chitosan, (b) CHGC, (c) PCP, and (d) PCP-CHGC.

to the distal end of CHGC in the presence of SMCC, which is a heterobifunctional cross-linking reagent incorporating an extended spacer with amine and sulfhydryl reactivity. Compared with the ^{1}H NMR spectrum of CHGC, PCP-CHGC exhibited principal peaks related to the PCP moieties (4.16, 3.23, 3.10, 1.55, 1.16, and 0.87 ppm). These results revealed that PCP-CHGC was successfully synthesized. Moreover, Ellman's assay was used to determine the amount of PCP group conjugated on the glycol chitosan backbone. The degree of substitution was 5.2 PCP groups per 100 sugar residues of glycol chitosan.

3.2. Characterization of Blank Micelles. The synthesized PCP-CHGC was able to self-assemble to form micelles in aqueous

Table 1: Physicochemical properties of drug-free and DOX-loaded micelles.

Sample	DOX/carrier[a]	Size (nm)[b]	PDI[c]	LC (%)[d]	EE (%)[e]
CHGC	—	228 ± 19.1	0.283 ± 0.056	—	—
PCP-CHGC	—	246 ± 20.4	0.276 ± 0.063	—	—
DOX-CHGC	1.5/10	274 ± 23.0	0.234 ± 0.053	10.5 ± 0.73	81.8 ± 9.34
DOX-PCP-CHGC	1.5/10	293 ± 22.5	0.289 ± 0.087	11.4 ± 0.48	85.8 ± 4.07

[a]The ratio of DOX to carrier, based on feed amount (mg/mg). [b]Measured by dynamic light scattering. [c]Polydispersity index. [d]Loading content. [e]Encapsulation efficiency. The results represent the mean ± SD ($n = 3$).

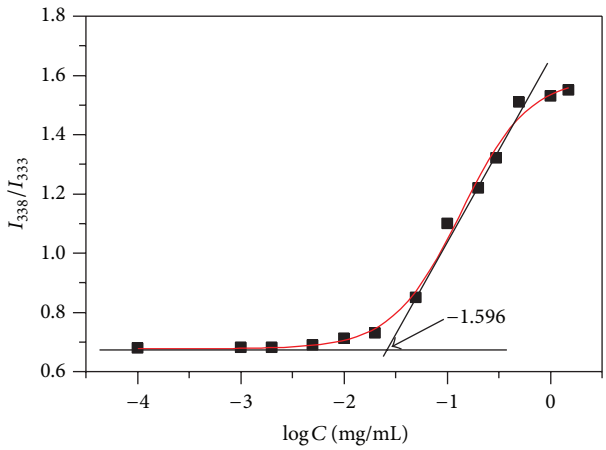

Figure 3: Plot of the intensity ratio I_{338}/I_{333} (from pyrene excitation spectra of PCP-CHGC conjugate) as a function of log C.

solution. As shown in Table 1, the mean diameters of CHGC and PCP-CHGC micelles analyzed by DLS were 228 and 246 nm, respectively. This result indicated that particle size of PCP-CHGC micelles increased after the modification of PCP groups on the outer shell of micelles.

The CAC of PCP-CHGC copolymer was detected by fluorescence spectrophotometry with pyrene as a fluorescent probe. As shown in Figure 3, the value of I_{338}/I_{333} ratio was changed with increasing concentrations of the conjugate. It indicated that pyrene molecules were transferred from a water environment to a hydrophobic micellar microdomain [37]. The CAC of PCP-CHGC measured by fluorescence spectrometry was 0.0254 mg/mL, which suggested that PCP-CHGC micelles can form nanosized nanoparticles under highly diluted condition.

3.3. Preparation and Characterization of Drug-Loaded Micelles. The physical entrapment of DOX into polymeric micelles was achieved by an emulsion/solvent evaporation method. Triethylamine was used to remove hydrochloride from DOX·HCl [38]. In aqueous medium, DOX-PCP-CHGC micelles can be formed. CHGC and PCP-CHGC micelles showed good loading capacities for DOX (Table 1). The loading content of DOX-CHGC and DOX-PCP-CHGC micelles was 10.5% and 11.4%, respectively. This result indicated that the modification of PCP in PCP-CHGC micelles showed no significant effect on the drug loading into micelles ($P > 0.05$). Additionally, the encapsulation efficiency of DOX-CHGC and DOX-PCP-CHGC micelles was >80%, suggesting the good loading behavior of these polymeric micelles.

The particle size of DOX-loaded micelles was shown in Table 1. The mean diameters of DOX-CHGC and DOX-PCP-CHGC micelles were 274 and 293 nm, respectively. We noted that the size of DOX-loaded micelles was larger than that of drug-free micelle counterparts. This result was ascribed to the fact that DOX molecules were loaded into the micellar inner space. As shown in Figure 4, it is evident that the DOX-PCP-CHGC micelles are in a regular spherical shape. The mean diameter of DOX-PCP-CHGC micelles determined by TEM was about 240 nm, which was smaller than hydrodynamic size analyzed by DLS. This is due to the solvent effect. The particles size observed by TEM is the diameter of air-dried micelles, whereas the size measured by DLS is the hydrodynamic diameter of micelles in the hydrated state. Similar phenomena were also described in other literatures [39, 40].

3.4. In Vitro Drug Release. As shown in Figure 5, DOX from DOX-loaded micelles *in vitro* was investigated in PBS (pH 7.4). The cumulative DOX release from DOX-CHGC and DOX-PCP-CHGC micelles over 72 h was 50.4% and 49.1%, respectively. It was seen that DOX-CHGC and DOX-PCP-CHGC micelles exhibited similar release behavior. The PCP conjugation did not have significant effect on the release behavior of DOX-PCP-CHGC micelles. Moreover, DOX released was in a biphasic way, which showed an initial fast release at the first 6 h and was followed by a step of sustained release for up to 72 h. As previously described, the initial moderately fast release and sustained release drug system

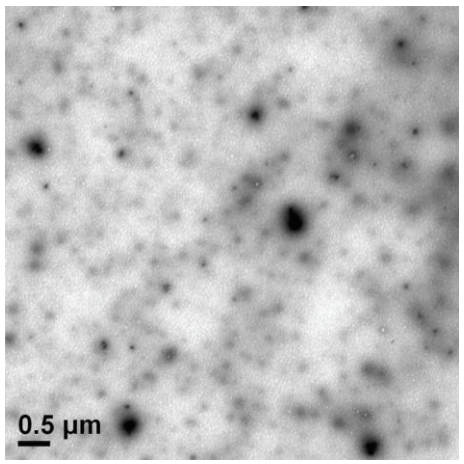

Figure 4: TEM image of DOX-PCP-CHGC micelles (×20000).

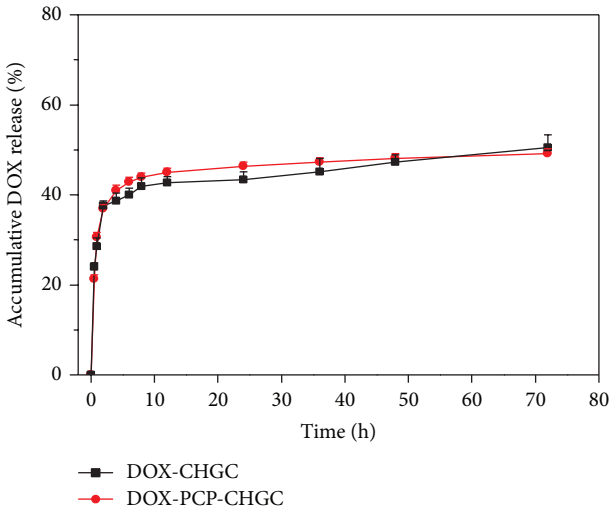

Figure 5: Release profiles of DOX from DOX-CHGC and DOX-PCP-CHGC micelles at 37°C in PBS at pH 7.4.

may offer the advantage of rapid drug effect and prolonged drug activity on the tumor [41]. Additionally, this release kinetic is related to both dissolution and diffusion based on the Noyes-Whitney law of dissolution and Fick's first law of diffusion [42].

3.5. In Vitro Cellular Uptake Study. The cellular uptake and distribution of micelles were monitored under CLSM and flow cytometry. As shown in Figure 6, the red fluorescence originated from DOX formulations. After incubating PSMA-positive LNCaP cells with DOX-CHGC or DOX-PCP-CHGC micelles for 4 h, the weak DOX fluorescence in cytoplasm was observed. In addition, the majority of visible red fluorescence was found in nuclei. It can be ascribed to the released DOX from the micelles. These results indicated that the micelles were taken by LNCaP cells through endocytosis. Moreover, the red fluorescence from the internalized DOX-PCP-CHGC was apparently brighter than that from DOX-CHGC, indicating that the cellular uptake for DOX-PCP-CHGC micelles was enhanced by PCP modification at the surface of micelles. It should also be noted that stronger DOX fluorescence was observed in the cells following incubation with free DOX·HCl, compared with DOX-CHGC and DOX-PCP-CHGC micelles. This result was due to the different internalization mechanisms of the DOX-loaded micelles and DOX·HCl. The DOX-loaded micelles were internalized through an endocytosis pathway, whereas DOX·HCl molecules were transported into the cells in a passive diffusion manner [43, 44]. DOX molecules from the micelles diffused into the cells more slowly than DOX·HCl in solution without micelle encapsulation.

To further determine the cellular uptake of DOX·HCl, DOX-CHGC, and DOX-PCP-CHGC micelles by LNCaP cells after 4 h incubation, flow cytometry was applied. As shown in Figure 7, the highest amount of cell-associated fluorescence was observed in LNCaP cells that had been incubated with DOX·HCl. The mean fluorescence intensities of DOX-CHGC, DOX-PCP-CHGC, and DOX·HCl were 69.26, 95.70, and 111.90, respectively. The cells incubated with DOX-PCP-CHGC micelles emitted higher fluorescent intensity

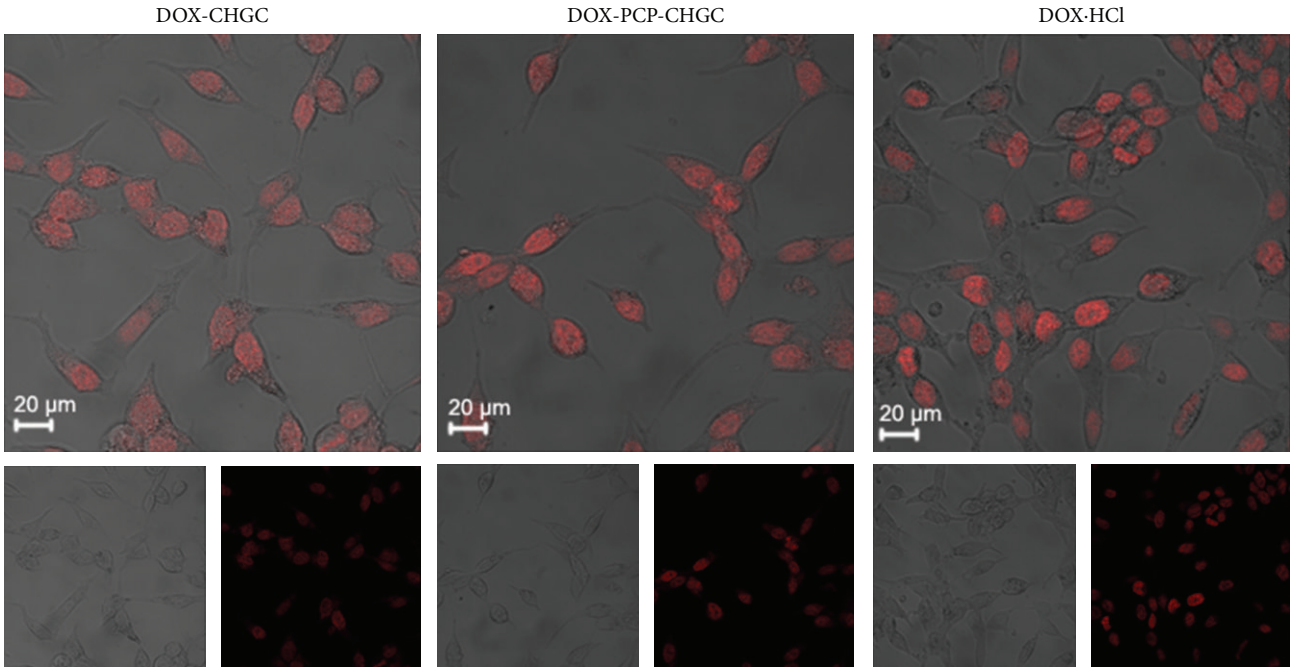

Figure 6: CLSM images of LNCaP cells after incubation with DOX·HCl, DOX-CHGC, or DOX-PCP-CHGC micelles for 4 h.

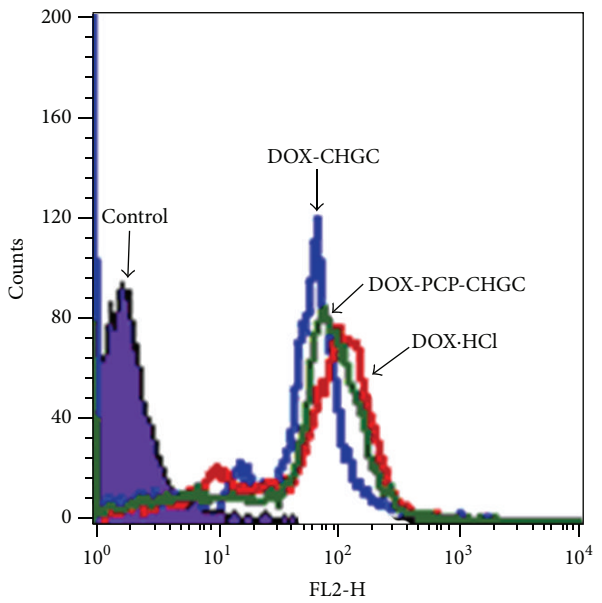

Figure 7: Flow cytometric analysis of LNCaP cells treated with DOX·HCl, DOX-CHGC, or DOX-PCP-CHGC micelles for 4 h.

than the cells treated with DOX-CHGC micelles. These results were in good agreement with those of CLSM experiments. Therefore, the PCP-conjugated micelles exhibited enhanced cellular uptake in LNCaP cells *in vitro* compared to nonconjugated micelles. This result indicated that PCP-modified micelles could facilitate and improve cellular uptake of micelles in tumor tissues.

3.6. In Vitro Cytotoxicity. *In vitro* cytotoxic activity of DOX-loaded micelles against LNCaP (PSMA+) and PC-3 (PSMA−) cells was evaluated by using MTT assay. Figure 8(a) demonstrates the survival rates of DOX·HCl, DOX-CHGC, and DOX-PCP-CHGC under a series of DOX concentrations against PC-3 cells. The results show that these DOX formulations can inhibit the cells' growth in a dose-dependent manner. The 50% inhibitory concentration (IC_{50}) of DOX·HCl, DOX-CHGC, and DOX-PCP-CHGC was 13.12, 13.32, and 19.18 μg/mL, respectively. DOX·HCl exhibited stronger cytotoxicity compared with DOX-CHGC and DOX-PCP-CHGC. Similarly, Xie et al. reported that the cytotoxicity

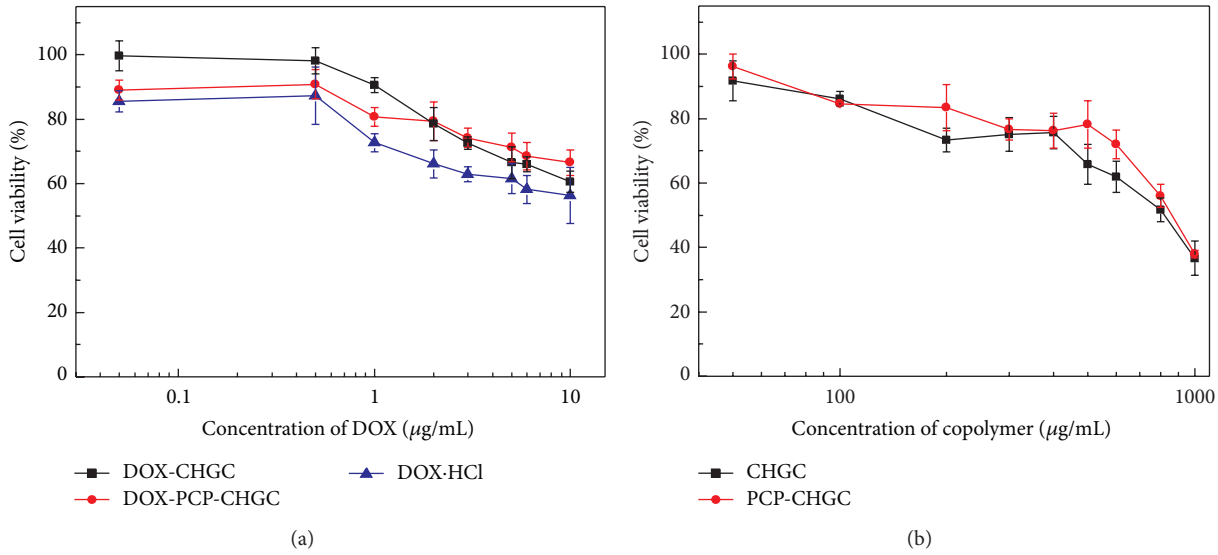

FIGURE 8: The *in vitro* cytotoxicity of (a) DOX·HCl, DOX-CHGC, DOX-PCP-CHGC, and (b) CHGC and PCP-CHGC micelles against PC-3 cells after 24-hour incubation.

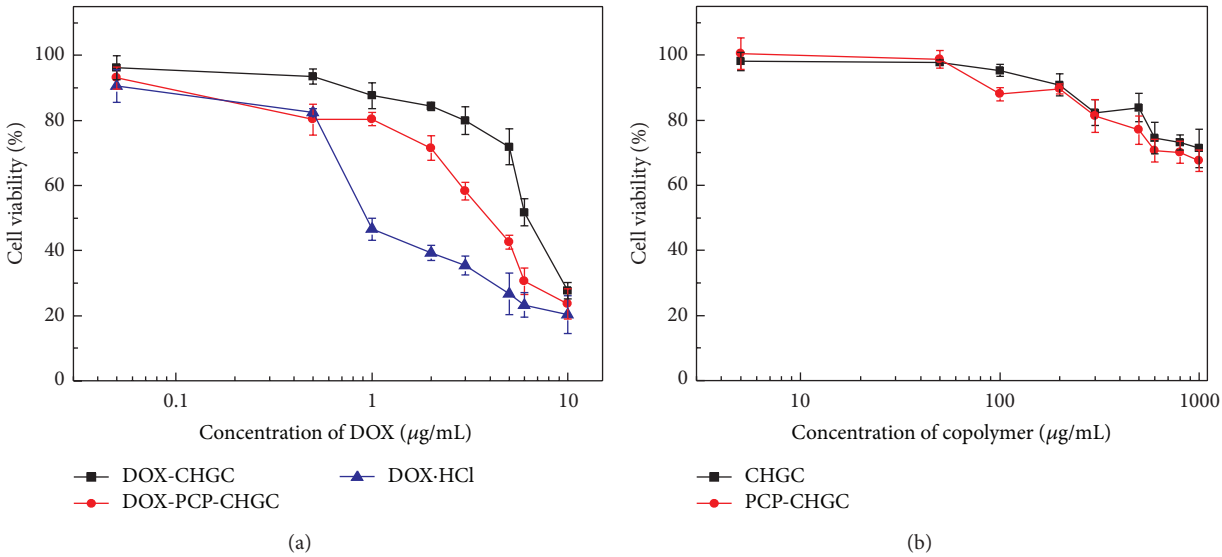

FIGURE 9: The *in vitro* cytotoxicity of (a) DOX·HCl, DOX-CHGC, DOX-PCP-CHGC, and (b) CHGC and PCP-CHGC micelles against LNCaP cells after 24-hour incubation.

of DOX-loaded CS-SA micelles against C6 cells was less potent than that of DOX·HCl [45]. This is due to the fact that DOX·HCl could be quickly delivered into cells by passive diffusion and instantly inhibit cell growth under the *in vitro* condition. Moreover, we can see that the cytotoxicity of DOX-PCP-CHGC is lower than that of DOX-CHGC. This result demonstrated that DOX-PCP-CHGC with PCP modifications could not perform the targeting capability in PSMA-negative PC-3 cells. As shown in Figure 8(b), the IC_{50} values of blank CHGC and PCP-CHGC micelles were 870.1 and 983.1 μg/mL, respectively. These results revealed that these blank micelles showed low cytotoxicity against the test cells.

The cytotoxicity of three DOX formulations against LNCaP cells for 24 h was shown in Figure 9(a). The IC_{50} of DOX·HCl was 1.37 μg/mL, while that of DOX-CHGC and DOX-PCP-CHGC micelles at the equivalent DOX concentration was 6.82 and 3.48 μg/mL, respectively. DOX-loaded micelles revealed lower cell killing efficiency as compared to DOX·HCl. DOX-PCP-CHGC micelles showed significantly greater cell killing potency against LNCaP cells in contrast with DOX-CHGC micelles ($P < 0.05$). The decoration of PCP molecules on the micelles could help to enhance their recognition to LNCaP tumor cells and to facilitate intracellular drug delivery through the PSMA-mediated endocytosis, leading to the increase of cytotoxicity of DOX-PCP-CHGC

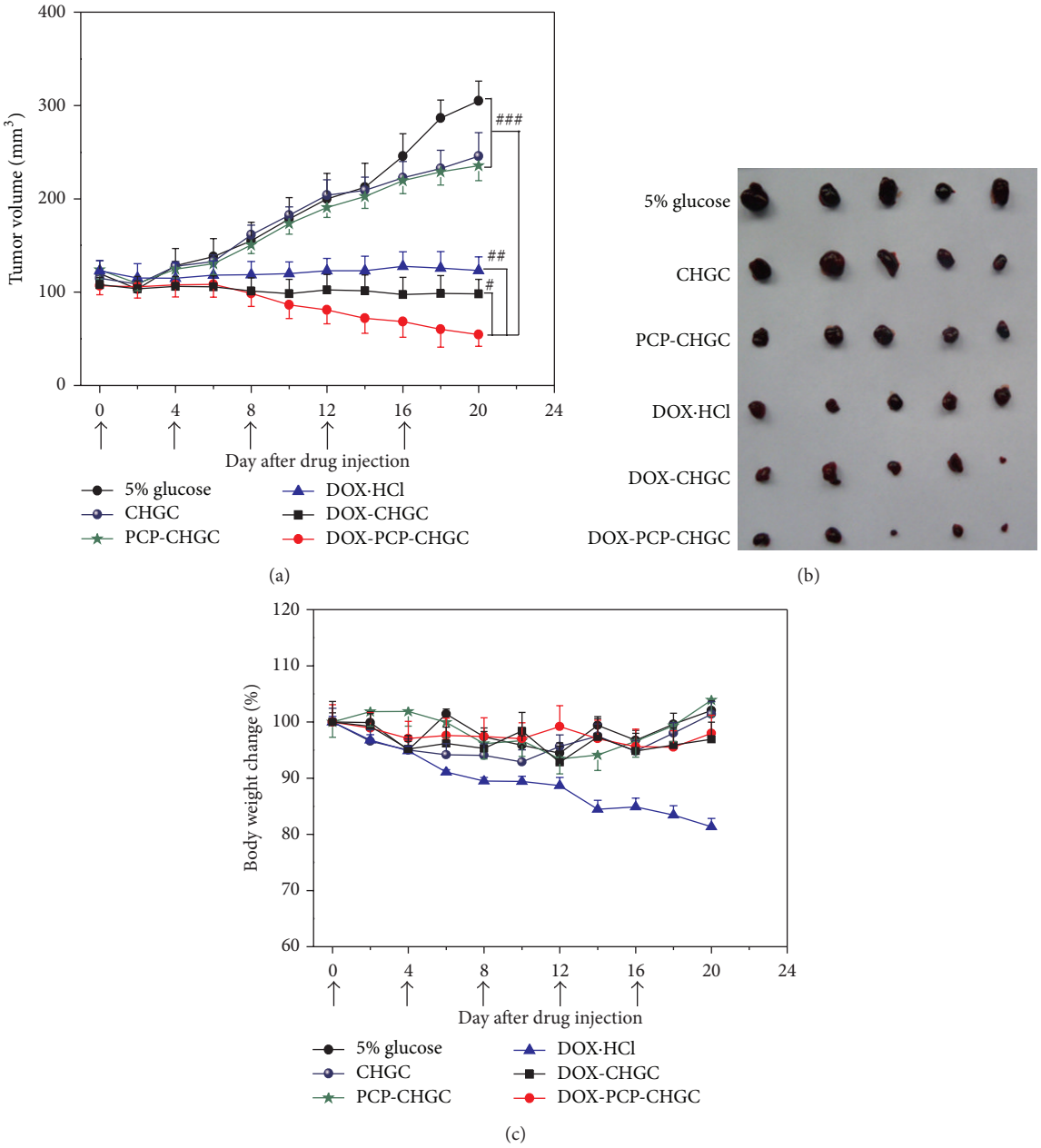

FIGURE 10: *In vivo* antitumor activity of 5% glucose, DOX·HCl, CHGC, PCP-CHGC, DOX-CHGC, and DOX-PCP-CHGC micelles in LNCaP-bearing nude mice: (a) mice tumor volume, (b) images of LNCaP xenograft tumors after treatment on 20th day, and (c) mice body weight changed within 20 days. Arrows represent drug administration. Data represented as mean ± SD ($n = 5$). $^{\#}P < 0.05$, $^{\#\#}P < 0.01$, $^{\#\#\#}P < 0.001$.

micelles. These results agreed well with the cellular uptake study. Notably, it was unlikely that such a high concentration of DOX·HCl would be present in the tumor site during the blood circulation *in vivo*. And DOX-loaded micelles may facilitate its accumulation at tumor tissue by the EPR effect as previously described [31, 43]. For comparison, the cytotoxicity of the empty micelles was also investigated. As shown in Figure 9(b), the viability of empty CHGC and PCP-CHGC micelles against LNCaP cells after 24-hour treatment was nearly 70% even at high concentration of 1 mg/mL. This result exhibited that empty micelles had good biocompatibility. Therefore, we inferred that PCP-modified micelles could be a potential carrier for PSMA-mediated targeting drug delivery.

3.7. In Vivo Tumor Inhibition Study. In order to validate the ability of PCP-modified nanoparticles to target tumors *in vivo*, the antitumor efficacy of DOX-PCP-CHGC micelles was further verified using BALB/C nude mice bearing LNCaP cancer xenografts. As shown in Figure 10(a), DOX·HCl, DOX-CHGC, and DOX-PCP-CHGC groups demonstrated significant tumor inhibition to different levels. At day 20 after the first treatment, the mean tumor volumes of DOX·HCl,

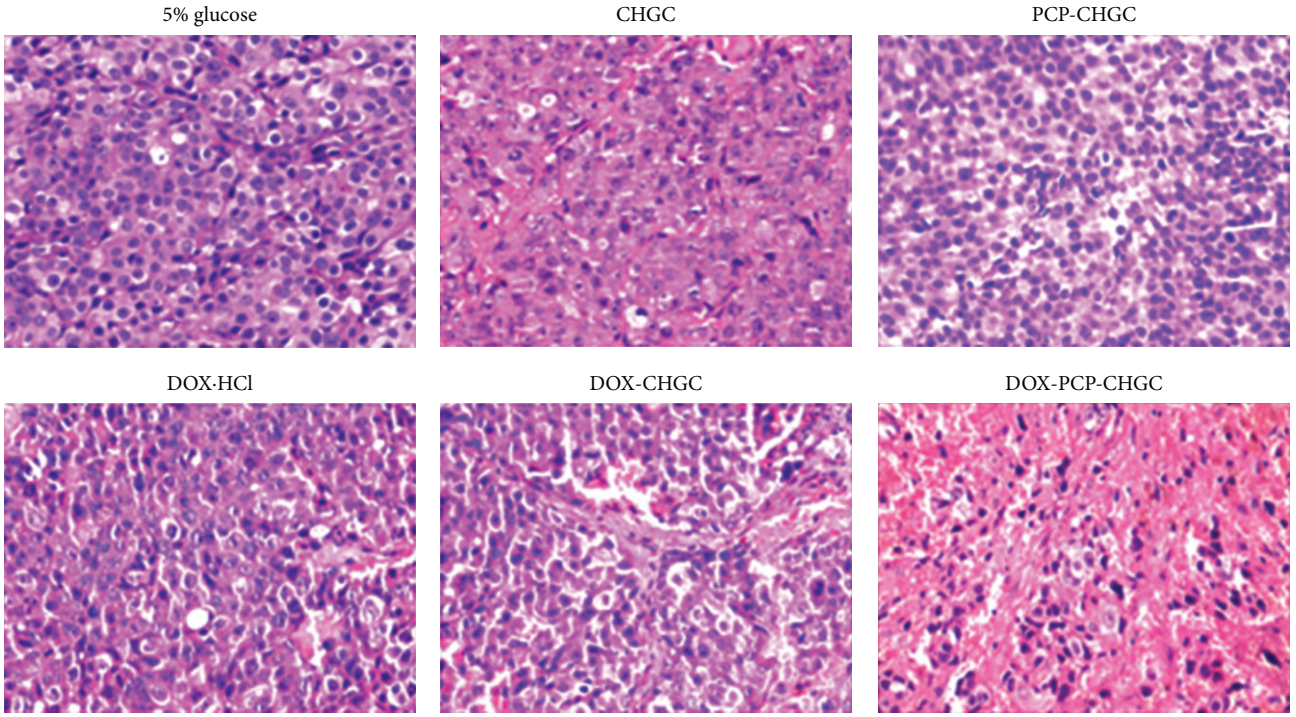

Figure 11: Light microscopy images of H&E staining LNCaP tumors after treatment on 20th day (×200).

DOX-CHGC, and DOX-PCP-CHGC groups were 123.3, 98.2, and 54.5 mm^3, respectively. Therefore, DOX-PCP-CHGC exhibited outstanding antitumor activity compared with DOX·HCl and DOX-CHGC group ($P < 0.05$ versus DOX-CHGC, and $P < 0.01$ versus DOX·HCl). These results demonstrated that PCP-modified micelles could improve DOX delivery into LNCaP tumors by PSMA-mediated active targeting. Moreover, the tumor volume of DOX-CHGC group was smaller than that of DOX·HCl group, indicating that the antitumor activity of DOX-loaded micelles was enhanced by the EPR effect. Additionally, the tumor volume of mice in 5% glucose, CHGC and PCP-CHGC groups rapidly increased and exhibited significant differences ($P < 0.001$) in contrast with DOX-PCP-CHGC group. Interestingly, the most tumor inhibition was found in the group that was treated with DOX-PCP-CHGC. From the data of cellular uptake *in vitro* (Figures 6 and 7), it was shown that enhanced intracellular accumulation of DOX was observed with the treatment of DOX-PCP-CHGC in contrast to DOX-CHGC. And DOX·HCl group exhibited the strongest cellular uptake *in vitro*. As previously reported, free DOX showed rapid clearance from rat plasma [20]. However, DOX encapsulated in the polymeric nanoparticles exhibited delayed blood clearance. The long-circulating characteristic of the polymeric nanoparticles endows EPR effect more valuable in tumor targeting [11]. Therefore, the EPR effect in solid tumors could contribute to the enhanced antitumor activity of DOX-loaded polymeric micelles. Furthermore, improved tumor targeting of *in vivo* DOX delivery was seen in the PCP-modified micelles when compared to that of nontargeted micelles. These results indicated that administration of DOX-PCP-CHGC could accumulate in the same tumor tissues with PSMA-mediated pattern.

At the end of the experiment, the images of isolated tumors for different treated groups confirmed the superior efficiency of DOX-PCP-CHGC micelles (Figure 10(b)). Meanwhile, the body weight of mice was monitored to evaluate the systemic toxicity of the formulations during the experiment. As shown in Figure 10(c), the treated mice except DOX·HCl group exhibited a slight weight change. This might be due to the bearing of tumor. Compared with DOX-loaded micelles groups, an apparent weight decrease was observed in DOX·HCl group. It inferred that DOX·HCl could not specifically deliver into the tumor cells, and the drug produced the side effects.

To further assess the therapeutic efficacy, histological analysis of tumor sections was performed on the 20th day after the first injection. From the H&E staining in Figure 11, we can find that, in comparison with 5% glucose, blank micelle, DOX·HCl and DOX-CHGC groups, DOX-PCP-CHGC group exhibited the greatest massive cancer cell remission and distinct apoptosis degrees. Therefore, DOX-PCP-CHGC micelles could provide better antitumor efficiency with low side effects by enhancing accumulation in tumors and improve cellular uptake.

4. Conclusion

In the present work, novel PCP-CHGC copolymer was successfully synthesized and characterized. DOX was physically encapsulated into PCP-CHGC micelles with high drug-loading capacity. *In vitro* cytotoxicity and cellular uptake studies revealed that the PCP-modified micelles could specifically recognize the PSMA-positive LNCaP cells and enhance

intracellular DOX delivery by PSMA-mediated endocytosis. Furthermore, DOX-PCP-CHGC micelles demonstrated better tumor inhibition in LNCaP-bearing nude mice than DOX·HCl and DOX-CHGC micelles. These findings suggested that this formulation design provided promising targeted therapeutics for PSMA-expressing prostate cancer.

Conflict of Interests

The authors declare that there is no conflict of interests regarding the publication of this paper.

Acknowledgments

This work was financially supported by the Natural Science Foundation of Jiangxi Province (no. 20114BAB215017) and the National Nature Science Foundation of China (no. 81360484). Jing Xu, M.S. degree candidate, is grateful to Dr. Huan Yu for her helpful comments.

References

[1] R. Siegel, J. Ma, Z. Zou, and A. Jemal, "Cancer statistics, 2014," *CA: A Cancer Journal for Clinicians*, vol. 64, no. 1, pp. 9–29, 2014.

[2] Z. H. Peng, M. Sima, M. E. Salama, P. Kopeckova, and J. Kopecek, "Spacer length impacts the efficacy of targeted docetaxel conjugates in prostate-specific membrane antigen expressing prostate cancer," *Journal of Drug Targeting*, vol. 21, no. 10, pp. 968–980, 2013.

[3] B. Qin, W. Tai, R. S. Shukla, and K. Cheng, "Identification of a LNCaP-specific binding peptide using phage display," *Pharmaceutical Research*, vol. 28, no. 10, pp. 2422–2434, 2011.

[4] Y. Barenholz, "Doxil—the first FDA-approved nano-drug: lessons learned," *Journal of Controlled Release*, vol. 160, no. 2, pp. 117–134, 2012.

[5] J. Pan, Y. Liu, and S.-S. Feng, "Multifunctional nanoparticles of biodegradable copolymer blend for cancer diagnosis and treatment," *Nanomedicine*, vol. 5, no. 3, pp. 347–360, 2010.

[6] J. Hu, S. Miura, K. Na, and Y. H. Bae, "pH-responsive and charge shielded cationic micelle of poly(L-histidine)-*block*-short branched PEI for acidic cancer treatment," *Journal of Controlled Release*, vol. 172, no. 1, pp. 69–76, 2013.

[7] J. Ding, J. Chen, D. Li et al., "Biocompatible reduction-responsive polypeptide micelles as nanocarriers for enhanced chemotherapy efficacy in vitro," *Journal of Materials Chemistry B*, vol. 1, no. 1, pp. 69–81, 2013.

[8] R. Luxenhofer, A. Schulz, C. Roques et al., "Doubly amphiphilic poly(2-oxazoline)s as high-capacity delivery systems for hydrophobic drugs," *Biomaterials*, vol. 31, no. 18, pp. 4972–4979, 2010.

[9] M. Shahin, S. Ahmed, K. Kaur, and A. Lavasanifar, "Decoration of polymeric micelles with cancer-specific peptide ligands for active targeting of paclitaxel," *Biomaterials*, vol. 32, no. 22, pp. 5123–5133, 2011.

[10] N. V. Cuong, M. F. Hsieh, Y. T. Chen, and I. Liau, "Doxorubicin-loaded nanosized micelles of a star-shaped poly(ε-caprolactone)-polyphosphoester block co-polymer for treatment of human breast cancer," *Journal of Biomaterials Science, Polymer Edition*, vol. 22, no. 11, pp. 1409–1426, 2011.

[11] Y. Matsumura and H. Maeda, "A new concept for macromolecular therapeutics in cancer chemotherapy: mechanism of tumoritropic accumulation of proteins and the antitumor agent smancs," *Cancer Research*, vol. 46, no. 12, pp. 6387–6392, 1986.

[12] N. Wiradharma, Y. Zhang, S. Venkataraman, J. L. Hedrick, and Y. Y. Yang, "Self-assembled polymer nanostructures for delivery of anticancer therapeutics," *Nano Today*, vol. 4, no. 4, pp. 302–317, 2009.

[13] V. Torchilin, "Tumor delivery of macromolecular drugs based on the EPR effect," *Advanced Drug Delivery Reviews*, vol. 63, no. 3, pp. 131–135, 2011.

[14] J.-H. Kim, Y.-S. Kim, K. Park et al., "Self-assembled glycol chitosan nanoparticles for the sustained and prolonged delivery of antiangiogenic small peptide drugs in cancer therapy," *Biomaterials*, vol. 29, no. 12, pp. 1920–1930, 2008.

[15] S. Kwon, J. H. Park, H. Chung, I. C. Kwon, S. Y. Jeong, and I.-S. Kim, "Physicochemical characteristics of self-assembled nanoparticles based on glycol chitosan bearing 5 β-cholanic acid," *Langmuir*, vol. 19, no. 24, pp. 10188–10193, 2003.

[16] J.-H. Kim, S. M. Bae, M.-H. Na et al., "Facilitated intracellular delivery of peptide-guided nanoparticles in tumor tissues," *Journal of Controlled Release*, vol. 157, no. 3, pp. 493–499, 2012.

[17] Y. J. Son, J.-S. Jang, Y. W. Cho et al., "Biodistribution and anti-tumor efficacy of doxorubicin loaded glycol-chitosan nanoaggregates by EPR effect," *Journal of Controlled Release*, vol. 91, no. 1-2, pp. 135–145, 2003.

[18] H. S. Yoo, J. E. Lee, H. Chung, I. C. Kwon, and S. Y. Jeong, "Self-assembled nanoparticles containing hydrophobically modified glycol chitosan for gene delivery," *Journal of Controlled Release*, vol. 103, no. 1, pp. 235–243, 2005.

[19] S. J. Lee, K. Park, Y.-K. Oh et al., "Tumor specificity and therapeutic efficacy of photosensitizer-encapsulated glycol chitosan-based nanoparticles in tumor-bearing mice," *Biomaterials*, vol. 30, no. 15, pp. 2929–2939, 2009.

[20] J.-M. Yu, Y.-J. Li, L.-Y. Qiu, and Y. Jin, "Polymeric nanoparticles of cholesterol-modified glycol chitosan for doxorubicin delivery: preparation and in-vitro and in-vivo characterization," *Journal of Pharmacy and Pharmacology*, vol. 61, no. 6, pp. 713–719, 2009.

[21] R. R. Sawant, A. M. Jhaveri, A. Koshkaryev, F. Qureshi, and V. P. Torchilin, "The effect of dual ligand-targeted micelles on the delivery and efficacy of poorly soluble drug for cancer therapy," *Journal of Drug Targeting*, vol. 21, no. 7, pp. 630–638, 2013.

[22] Y. Miura, T. Takenaka, K. Toh et al., "Cyclic RGD-linked polymeric micelles for targeted delivery of platinum anticancer drugs to glioblastoma through the blood-brain tumor barrier," *ACS Nano*, vol. 7, no. 10, pp. 8583–8592, 2013.

[23] C. Zhan, B. Li, L. Hu et al., "Micelle-based brain-targeted drug delivery enabled by a nicotine acetylcholine receptor ligand," *Angewandte Chemie—International Edition*, vol. 50, no. 24, pp. 5482–5485, 2011.

[24] B. Xiang, D.-W. Dong, N.-Q. Shi et al., "PSA-responsive and PSMA-mediated multifunctional liposomes for targeted therapy of prostate cancer," *Biomaterials*, vol. 34, no. 28, pp. 6976–6991, 2013.

[25] E. Kim, Y. Jung, H. Choi et al., "Prostate cancer cell death produced by the co-delivery of Bcl-xL shRNA and doxorubicin using an aptamer-conjugated polyplex," *Biomaterials*, vol. 31, no. 16, pp. 4592–4599, 2010.

[26] S. Hwa Kim, S. Hyeon Lee, H. Tian, X. Chen, and T. Gwan Park, "Prostate cancer cellspecific VEGF siRNA delivery system using cell targeting peptide conjugated polyplexes," *Journal of Drug Targeting*, vol. 17, no. 4, pp. 311–317, 2009.

[27] A. Ghosh and W. D. W. Heston, "Tumor target prostate specific membrane antigen (PSMA) and its regulation in prostate cancer," *Journal of Cellular Biochemistry*, vol. 91, no. 3, pp. 528–539, 2004.

[28] H.-W. Yang, M.-Y. Hua, H.-L. Liu et al., "Cooperative dual-activity targeted nanomedicine for specific and effective prostate cancer therapy," *ACS Nano*, vol. 6, no. 2, pp. 1795–1805, 2012.

[29] S. F. Slovin, "Targeting novel antigens for prostate cancer treatment: focus on prostate-specific membrane antigen," *Expert Opinion on Therapeutic Targets*, vol. 9, no. 3, pp. 561–570, 2005.

[30] V. I. Romanov, D. B. Durand, and V. A. Petrenko, "Phage display selection of peptides that affect prostate carcinoma cells attachment and invasion," *Prostate*, vol. 47, no. 4, pp. 239–251, 2001.

[31] J. Yu, X. Xie, X. Xu et al., "Development of dual ligand-targeted polymeric micelles as drug carriers for cancer therapy *in vitro* and *in vivo*," *Journal of Materials Chemistry B*, vol. 2, no. 15, pp. 2114–2126, 2014.

[32] J. Yu, X. Xie, M. Zheng et al., "Fabrication and characterization of nuclear localization signal-conjugated glycol chitosan micelles for improving the nuclear delivery of doxorubicin," *International Journal of Nanomedicine*, vol. 7, pp. 5079–5090, 2012.

[33] Y.-Z. Du, L. Wang, H. Yuan, X.-H. Wei, and F.-Q. Hu, "Preparation and characteristics of linoleic acid-grafted chitosan oligosaccharide micelles as a carrier for doxorubicin," *Colloids and Surfaces B: Biointerfaces*, vol. 69, no. 2, pp. 257–263, 2009.

[34] L. Y. Qiu and M. Q. Yan, "Constructing doxorubicin-loaded polymeric micelles through amphiphilic graft polyphosphazenes containing ethyl tryptophan and PEG segments," *Acta Biomaterialia*, vol. 5, no. 6, pp. 2132–2141, 2009.

[35] K. Kataoka, T. Matsumoto, M. Yokoyama et al., "Doxorubicin-loaded poly(ethylene glycol)-poly(β-benzyl-L-aspartate) copolymer micelles: their pharmaceutical characteristics and biological significance," *Journal of Controlled Release*, vol. 64, no. 1–3, pp. 143–153, 2000.

[36] J. Yu, X. Xie, J. Wu et al., "Folic acid conjugated glycol chitosan micelles for targeted delivery of doxorubicin: Preparation and preliminary evaluation *in vitro*," *Journal of Biomaterials Science, Polymer Edition*, vol. 24, no. 5, pp. 606–620, 2013.

[37] J. Zhang and P. X. Ma, "Polymeric core-shell assemblies mediated by host-guest interactions: versatile nanocarriers for drug delivery," *Angewandte Chemie International Edition*, vol. 48, no. 5, pp. 964–968, 2009.

[38] V. A. Sethuraman and Y. H. Bae, "TAT peptide-based micelle system for potential active targeting of anti-cancer agents to acidic solid tumors," *Journal of Controlled Release*, vol. 118, no. 2, pp. 216–224, 2007.

[39] X. Wang, X. Zhen, J. Wang, J. Zhang, W. Wu, and X. Jiang, "Doxorubicin delivery to 3D multicellular spheroids and tumors based on boronic acid-rich chitosan nanoparticles," *Biomaterials*, vol. 34, no. 19, pp. 4667–4679, 2013.

[40] L. Yan, W. Wu, W. Zhao et al., "Reduction-sensitive core-crosslinked mPEG-poly(ester-carbonate) micelles for glutathione-triggered intracellular drug release," *Polymer Chemistry*, vol. 3, no. 9, pp. 2403–2412, 2012.

[41] Y. W. Won, S. M. Yoon, K. S. Lim, and Y. H. Kim, "Self-assembled nanoparticles with dual effects of passive tumor targeting and cancer-selective anticancer effects," *Advanced Functional Materials*, vol. 22, no. 6, pp. 1199–1208, 2012.

[42] M. Barzegar-Jalali, K. Adibkia, H. Valizadeh et al., "Kinetic analysis of drug release from nanoparticles," *Journal of Pharmacy and Pharmaceutical Sciences*, vol. 11, no. 1, pp. 167–177, 2008.

[43] M. Li, Z. Tang, S. Lv et al., "Cisplatin crosslinked pH-sensitive nanoparticles for efficient delivery of doxorubicin," *Biomaterials*, vol. 35, no. 12, pp. 3851–3864, 2014.

[44] Y. Pu, S. Chang, H. Yuan, G. Wang, B. He, and Z. Gu, "The anti-tumor efficiency of poly(L-glutamic acid) dendrimers with polyhedral oligomeric silsesquioxane cores," *Biomaterials*, vol. 34, no. 14, pp. 3658–3666, 2013.

[45] Y. T. Xie, Y. Z. Du, H. Yuan, and F. Q. Hu, "Brain-targeting study of stearic acid-grafted chitosan micelle drug-delivery system," *International Journal of Nanomedicine*, vol. 7, pp. 3235–3244, 2012.